32nd EPS Conference on Plasma Phys. Tarragona, 27 June - 1 July 2005 ECA Vol.29C, P-2.010 (2005)

In situ Measurement of Chemical Erosion Yields for the Production of C_2H_y in the JET Outer Divertor

S. Brezinsek[1], M.F. Stamp[2], A. Pospieszczyk[1], A. Meigs[2], A. Huber[1], S. Jachmich[3], A. Kirschner[1], Ph. Mertens[1], V. Philipps[1], U. Samm[1], G.F. Matthews[2] and JET EFDA contributors*

[1]*Institut für Plasmaphysik, Forschungszentrum Jülich GmbH, EURATOM-Association, Trilateral Euregio Cluster, D-52425 Jülich, Germany*
[2]*EURATOM/UKAEA Fusion Association, Culham Science Centre, Oxon OX14 3DB, UK*
[3]*Laboratoire de Physique des Plasmas/Laboratorium voor Plasmafysica, ERM/KMS, EURATOM Association, Trilateral Euregio Cluster, B-1000 Brussels, Belgium*

1. Introduction

Graphite is currently planned for the high heat load areas of the ITER divertor targets. Erosion will determine both the lifetime of these components and the long term retention of tritium via the formation of hydrogen-rich carbon layers on remote areas and on the targets themselves. A reliable database exists for the chemical erosion yield Y_{chem} of graphite under the impact of energetic and thermal hydrogen in beam experiments, but although data describing the erosion behaviour of graphite targets in fusion devices has recently been compiled and critically revisited [1], no such detailed study exists for higher hydrocarbons. Previous measurements in the JET MKII-GB divertor [2] indicated similar carbon yields from CH_4 and C_2H_y. The strong dependence of $Y_{chem}^{C_2H_y}$ with the ion flux [1] could not be addressed in [2].

In JET, gas injection experiments in the MKII-SRP divertor were performed to determine the (molecular) carbon flux originating from chemical erosion and resulting in C_2H_y species. The injection allows the *in situ* calibration of photon fluxes emitted by the different hydrocarbon fragments along the dissociation chain [3] which are spectroscopically observed. The approach is to introduce ethene into the outer divertor plasma through gas injection modules (GIM) positioned circumferentially between the vertical target plates. A sweep of the outer strike point (OSP), indicated by three separatrix positions in fig. 1, places the injection location (GIM10) sequentially into the far scrape-off layer (SOL), near-SOL or private-flux region (PFR). Reference discharges with hydrogen injection were made in order to match the plasma parameters which are perturbed as a result of the hydrocarbon injection [2]. The discharges were adjusted by matching the central line-averaged density.

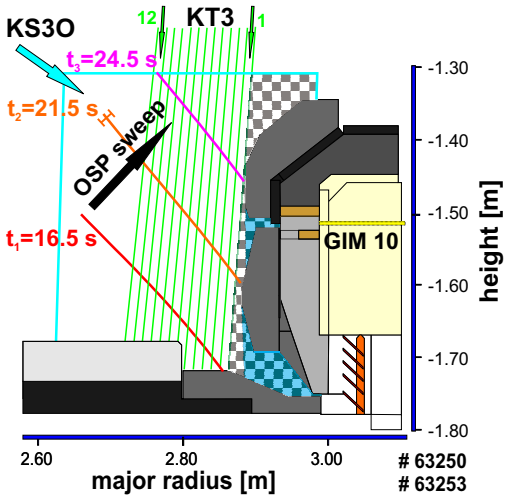

Figure 1: *Outer divertor: strike-point sweep and spectroscopic systems.*

The increase in the photon fluxes with respect to the reference discharge can be attributed to the injected C_2H_4. Effective photon efficiencies are estimated from the ratio between photon and particle fluxes, and they are applied to the intrinsic photon flux. The resulting C_2H_y particle flux is related to the hydrogen recycling flux and thus provides $Y_{chem}^{C_2H_y}$.

*See the Appendix of J.Pamela et al., Fusion Energy 2004 (Proc. 20th Int. Conf. Vilamoura, 2004) IAEA, Vienna (2004)

2. Experimental conditions and spectroscopic set-up

We performed high clearance L-mode discharges (hydrogen plasmas, 2.43 T, 2.5 MA, 3.4 MW NBI) with large and symmetric sweep of the strike points – starting from the horizontal target *ht* (t=18 s) and ending on the upper vertical target *vt* (t=24 s). A constant gas injection through GIM10 ($2.5*10^{21}$ C_2H_4 molecules/s) was made between 15 s and 25 s. Although the main plasma does not change significantly during the sweep, the plasma parameters at the injection location vary, reaching maximum values of T_e=22 eV and n_e=$5.5*10^{19}$ m^{-3} with peak ion fluxes of $1.65*10^{23}$ $s^{-1}m^{-2}$ at the target surface. These values were determined by Langmuir probes (LP) [4] – located close to GIM10 – while the profiles were mapped to the injection location. The T_e and n_e profiles for the injection and reference discharge are illustrated in fig. 2; they are well matched. The EFIT reconstruction of the magnetic topology was used to determine the separatrix and OSP position shown in fig. 1 and marked in fig. 2 with respect to the LP. The LP data indicate that the OSP of T_e and of n_e are slightly shifted. The difference in the OSP corresponds to half a second of the sweep or about 3 cm in vertical displacement.

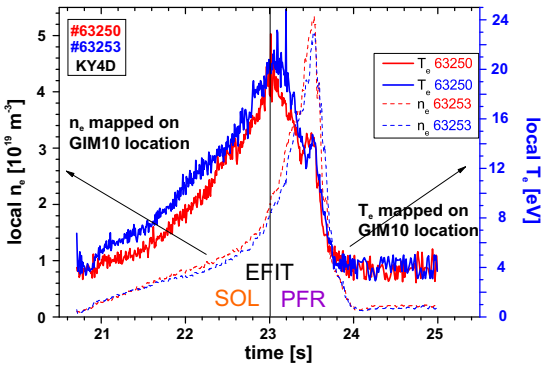

Figure 2: *Local T_e and n_e profiles.*

Three spectroscopic systems were used to observe the break-up of the injected C_2H_4: (i) the fibre-coupled survey spectrometer KS3 in the VIS [2] which provides an integral view of the outer divertor, (ii) the KT3 system [3] which provides radial information over 150 mm from the UV to the NIR, and (iii) the camera system KL1 [5] which is equipped with interference filters for CIII and H_α and used for tomographic reconstruction. Note that all systems have a restricted view in the corner as well as in a small region directly in front of the injection module (chequered areas in fig. 1). However, the increase in measured photon fluxes with respect to the reference discharge, e.g. shown in fig. 3 for C_2 (Swan-band), CII (514 nm), CIII (465 nm), can be attributed to the injected C_2H_4. The time period correlated to available LP data is highlighted in yellow.

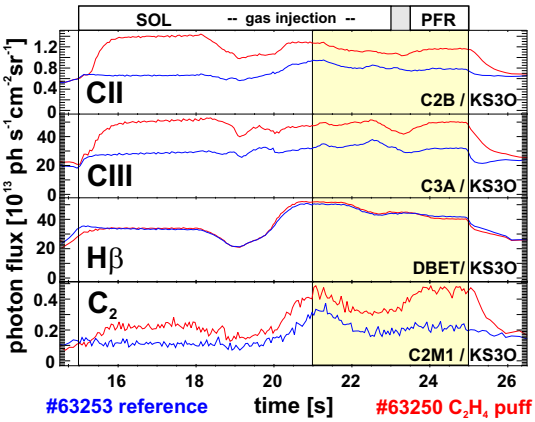

Figure 3: *Photon flux time evolution.*

3. Inverse photon efficiencies for C_2 and $Y_{chem}^{C_2H_y}$

Inverse photon efficiencies for C_2 from C_2H_4, or more precisely, $[D/XB]^{C_2<-C_2H_4}_{d-a,\ 515.2-516.5nm}$ values, take the dissociation chain into account and, thus, represent an effective value. Experimentally, these D/XB values have been determined in the following way:

$$\frac{D}{XB} = \frac{\Gamma^{GIM10}_{C_2H_4}}{\Delta\Phi^{inj.}_{C_2}} = \frac{\Gamma^{GIM10}_{C_2}}{\Phi^{inj.}_{C_2} - \Phi^{intr.}_{C_2}},$$

where $\Gamma^{GIM10}_{C_2H_4}$ represents the injected amount of ethene, $\Phi^{inj.}_{C_2}$ the C_2 photon flux during

the C_2H_4 injection, and $\Phi_{C_2}^{intr.}$ the intrinsic C_2 photon flux from the reference discharge. Φ_{C_2} is in both cases related to the bandhead of the *d-a* transition (515.2–516.5 nm). Assuming a toroidal homogeneity of the photon flux as well as of the injected particle flux, the total photon flux $[ph\ s^{-1}]$ was obtained by taking into account the outer divertor area of about 6.9 m^2. Fig. 3 shows that $\Phi_{C_2}^{inj.}$ is only twice as large as $\Phi_{C_2}^{intr.}$; this is typical of a circumferential injection and shows the difference to local injections ($\Phi_{C_2}^{inj.} \gg \Phi_{C_2}^{intr.}$). The photon flux for the complete electronic transition can be determined by applying a correction factor f, which takes the rovibrational population into account. For L-mode discharges, T_{rot} is about 4000 K [6] and $f \approx 15$.

The OSP sweep is equivalent to a variation of the plasma parameters at the injection location. Fig. 4a shows $[D/XB]^{C_2<-C_2H_4}_{d-a,\ 515.2-516.5\mathrm{nm}}$ as a function of the mapped n_e and T_e values. Two cases have to be distinguished: (i) injection into the SOL, the injected particles flow towards the separatrix where they will be ionised or dissociated, and (ii) injection into the PFR, the injected particles flow towards an open volume and can escape into the inner divertor. The later situation was observed here for t >23.5 s which coincides with the maximum of the n_e and ion density profile. In the following we assume that t=23.5 s determines the position in the sweep where the OSP is located at GIM10. D/XB values are no longer justified for t >23.5 s due to the loss of particles into the PFR (green-coloured area in fig. 4). For a comparison, the dotted lines indicate the position where according to the magnetic reconstruction the OSP is located on GIM10.

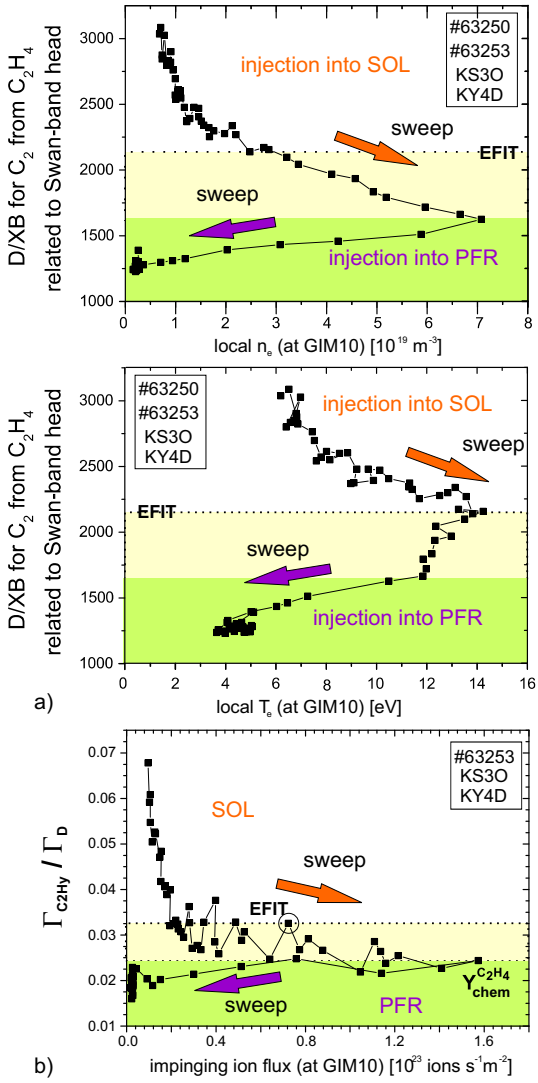

Figure 4: *a) D/XB for C_2 from C_2H_4. b) The erosion yield for C_2 from C_2H_y.*

Fig. 4a shows the dependence of the effective D/XB value on the local plasma parameters. In the first phase D/XB decreases strongly with increase of n_e and T_e down to 2200, while the decrease becomes less prominent for the next 0.5 s when T_e decreases but n_e still increases. The D/XB value is 1600 for the maximum ion flux. These values are higher then those reported in [7]. Applying the photon efficiencies to $\Phi_{C_2}^{intr.}$ provides the intrinsic particle flux $\Gamma_{C_2H_y}^{intr.}$, and the flux ratio with Γ_H, deduced from H_β and including a molecular correction [3], gives the chemical erosion yield for C_2H_y (fig. 4b). However, the conversion in $Y_{chem}^{C_2H_4}$ is most reliable at the location of the hydrocarbon source, which is – as we shall see – mainly at the location of highest ion flux. Finally, the D/XB values and the erosion yield present an upper limit, and both have to be reduced by approximately 25% due to

vignetting of the KS3 line of sight. Thus, we determine $Y_{chem}^{C_2H_y}$ to be at most 2% at the local surface temperature of about 450 K. Note that the erosion yield $Y_{chem}^{C_2H_y}$ determined in this experiment is comparable with the values given in [2].

4. Spatial distribution of the source

The time evolution of the radially resolved C_2 light pattern for the discharges with C_2H_4 injection (bottom) and H_2 injection (top) is depicted in fig. 5. Owing to the vignetting, KT3 is not able to provide information nearby the lower *vt*. Two general cases can be distinguished though. (i) The OSP is fixed on the *ht* and the light emission is concentrated in a few channels next to the OSP. (ii) The OSP is fixed on the *vt* and the light emission is smoothly spread over the whole outer divertor. The integral over all channels, and thus the hydrocarbon sources, for both cases are quite similar, but the distribution is completely different. The hydrocarbon injection modifies the light pattern only slightly, but changes the absolute values for both cases.

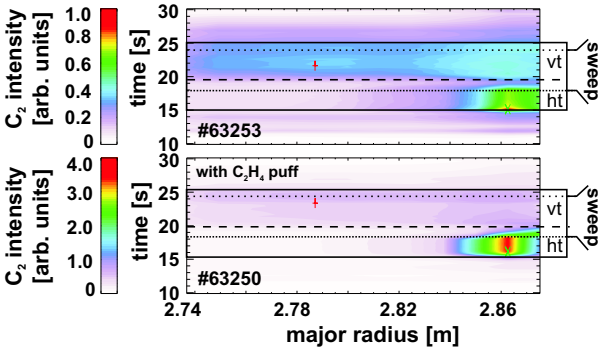

Figure 5: *Radial distribution of the C_2 photon flux in the outer divertor measured with KT3.*

The tomographic reconstruction of CIII and H_α for two different OSP positions is shown in fig. 6. Regarding the neutral species, H, the maximum emission is for both cases located near the OSP, but when the OSP is fixed on the vt an additional emission zone along the separatrix occurs. This second emission zone is even more pronounced in the case of the ionic species C^{2+}. Although no reconstruction for C_2 exists, one may apply this knowledge to C_2. The light emission along the separatrix may explain the smoothed and homogenous radial distribution of the C_2 Swan-band head. However, detailed modelling of the break-up chain is necessary to prove this.

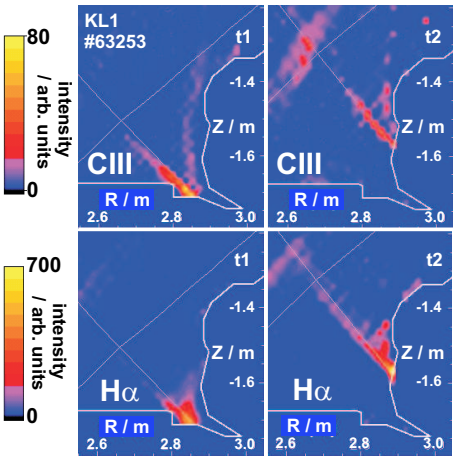

Figure 6: *Tomographic reconstruction: OSP on ht (left) and vt (right).*

5. Conclusion

The D/XB values for C_2H_4, their dependence on the local plasma parameters T_e and n_e, the light pattern of different break-up products and the upper limit for $Y_{chem}^{C_2H_4}$ of about 2% at a peak impinging ion flux of $1.65*10^{23}$ s^{-1} m^{-2} are the main results of the experiment presented here. These results have to be compared with simulations from the ERO code and will help to verify the code and the database for C_2H_y.

References

[1] J. Roth et al., *Nucl. Fusion* (2004), **44**, L21
[2] M.F. Stamp et al., *Physica Scripta* (2001), **T91**, 13
[3] S. Brezinsek et al., *Physica Scripta* (2004), **T111**, 42
[4] S. Jachmich et al., *28th EPS Contr. Fusion and Plasma Phys.* (2001), ECA Vol. 25A, 1617
[5] A. Huber et al., *Physica Scripta* (2004), **T111**, 101
[6] S. Brezinsek et al., *J. Nucl. Mater.* (2005), **337-339**, 1058
[7] A. Pospieszczyk et al., *UCLA-PPG report* (1989), **1251**